

**Supporting Information**

**Probing the nature and resistance of the molecule-electrode  
contact in SAM-based junctions**

*C. S. Suchand Sangeeth<sup>1</sup>, Albert Wan<sup>1</sup>, and Christian A. Nijhuis<sup>1,2\*</sup>*

<sup>1</sup> Department of Chemistry, National University of Singapore, 3 Science Drive 3,  
Singapore 117543.

<sup>2</sup> Centre for Advanced 2D Materials and Graphene Research Centre, 6 Science Drive  
2, Singapore 117546, Singapore.

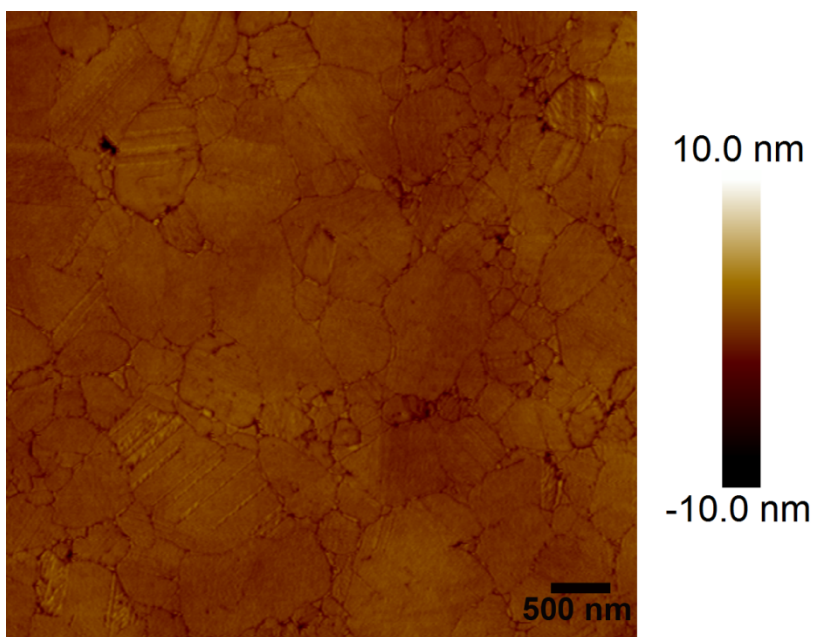
## **Experimental Details**

**Preparation of template-stripped Ag substrates.** We prepared the template-stripped Ag substrates by following a modified procedure that has been reported previously.<sup>1-4</sup> We thermally deposited a layer of 300 nm Ag (99.999% purity, purchased from Super Conductor Materials Inc, USA) on Si wafers (University wafers, USA) at a base pressure of  $\sim 2 \times 10^{-6}$  mbar in a thermal evaporator (ShenYang KeYi, China). The first 50 nm of Ag was deposited at a rate of 0.5-0.7 Å, and then another 250 nm was deposited of at a rate of  $\sim 1$  Å. We drop-casted thermally-curable epoxy (Epo-tek 353-ND 2-part epoxy-adhesive) on the Ag surfaces (instead of an optical adhesive as reported previously), followed by placing the substrates in a vacuum dessicator ( $\sim 500$  Torr) for 1 hour to remove the air bubbles from the epoxy. We cleaned glass slides (typically cut into pieces if  $1 \times 1$  cm<sup>2</sup>) by rinsing with ethanol (AR grade, Merck) and treated with oxygen plasma for 5 min at 500 mTorr; these glass slides were placed on the drop-casted epoxy on the Ag substrates. The epoxy was cured at 80 °C for 12 hours. To separate the Ag film supported on glass slides from the wafer, we cut the metal film around the sides of the glass support using a razor blade, and lifted the Ag-epoxy-glass substrate off from the wafer.

**Atomic Force Microscopy.** The atomic force microscopy (AFM) images of the bottom electrodes were recorded using Bruker Dimension FastScan AFM in tapping mode (FASTSCAN-A, resonant frequency: 1.4 MHz, force constant: 18 N/m) and the root mean square (rms) roughness are determined using the AFM software NanoScope Analysis (version 1.4).

**Characterization of the Ag<sup>TS</sup> surfaces.** Before we used the Ag<sup>TS</sup> surfaces, we characterized each new batch by AFM. Figure S1 shows a typical AFM image of the template-stripped Ag bottom electrode with a rms roughness of 0.6 nm over an area of 5×5 μm<sup>2</sup>. This image is very similar to previously reported results.<sup>2,5</sup>

**Figure S1.** AFM (5×5 μm<sup>2</sup>) image of the Ag<sup>TS</sup> surface.



**Purification of n-alkanethiolates.** The as received n-alkanethiolates (Sigma-Aldrich) were purified by recrystallization from absolute ethanol (AR grade) under atmospheric N<sub>2</sub> at -20 °C followed by filtration prior to use. Their purity was confirmed by <sup>1</sup>H NMR and GC-MS; these spectra were very similar to previously reported spectra.<sup>3,4</sup>

**Formation of SAMs.** We formed the SAMs from 3 mM ethanolic solutions of the corresponding n-alkanethiols (n = 10, 12, 14, 16, or 18) in an atmosphere of N<sub>2</sub> using previously reported procedures.<sup>2,3</sup> We only used freshly template-stripped Ag surfaces

and added them into the solution of the thiol of interest. We minimized the exposure of the Ag<sup>TS</sup> substrates to the ambient (usually less than 5 s) to avoid contamination. The SAMs were formed over three hours and then rinsed by ethanol and blown to dryness in a stream of N<sub>2</sub>.

**Fabrication of the Junctions.** We prepared a microfluidic chip which consists of GaO<sub>x</sub>/EGaIn injected within a channel connected with a through-hole (55 μm in diameter) following a previously reported method described in detail in reference <sup>3</sup>. First the EGaIn was injected in a channel (0.5 cm × 120 μm × 100 μm) that was aligned over the through-hole by applying EGaIn to the inlet and applying gentle vacuum (~500 Torr) to the outlet. During this step the EGaIn usually only filled the through-hole partially, if at all. A small second channel (0.5 cm × 10 μm × 20 μm; perpendicularly aligned with respect to the first channel) was also connected to the through-hole and was subjected to a gentle vacuum to force the EGaIn into the through-hole. The EGaIn did not fill the small second channel because of the high surface tension of EGaIn (624 mN/m).<sup>6, 7</sup> The GaO<sub>x</sub>/EGaIn confined within the PDMS through-hole served as the top-electrode with an area of the electrical contact of 9.6×10<sup>2</sup> μm<sup>2</sup>. We placed the top-electrode gently in contact with an Ag<sup>TS</sup> bottom-electrode that supported the SAMs for conducting the transport measurements. A drop of GaO<sub>x</sub>/EGaIn present at the inlet of the micro-channel was contacted with a tungsten probe while the bottom-electrode was grounded.<sup>3</sup>

**Charge transport measurements.** The  $J(V)$  measurements were carried out using a Keithley 6430 source meter and data were acquired using LabView 2010. We measured the impedance of these junctions using a Solartron impedance analyzer (model 1260A with 1296A dielectric interface which allows for two-terminal measurements) to obtain

the frequency profiles over the range of 1 Hz – 1 MHz by applying an AC voltage amplitude of 20 mV for junctions with  $n = 10$  or  $12$  and 30 mV for junction with  $n = 14$ , 16, or 18 superimposed on the desired DC bias in the range of  $\pm 0.5$  V in steps of 0.1 V. We found that for the junctions with thick SAMs with higher impedance, this small increase in the amplitude improved the signal-to-noise ratio significantly. We conducted the impedance measurements in reference mode using a standard 10 pF capacitor (model 12961 dielectric reference module) as the external reference. The reference mode measurements were needed to account for inductive effects due to the cables.<sup>8</sup> Using the same equipment, the temperature dependent impedance measurements were performed in a probe station (Lakeshore CRX-VF) at a pressure of  $3 \times 10^{-5}$  bar. We cooled down the probe station and then switched off the compressor during the impedance measurements to avoid electrical noise in the data. The temperature dependent impedance measurements were conducted in the frequency range 100 Hz – 1 MHz to reduce the measurement time and to improve the temperature stability (within 80 mK) during the measurement. This error in the temperature is small relative to the range of temperatures of 220 – 340 K, and 10 K intervals, which were measured.

**Data analysis.** The complex impedance is a more general concept than resistance because it considers both magnitude and phase of the applied sinusoidal signal (see for details reference 8). The complex impedance  $Z$  consists of real and imaginary parts and can be written as

$$Z = Z' + jZ'' \quad (S1)$$

with  $Z'$  is the real and  $Z''$  is the imaginary part. The modulus of the complex impedance  $|Z|$  can be calculated using the real and imaginary part as

$$|Z| = \sqrt{Z'^2 + Z''^2} \quad (\text{S2})$$

In polar form equation (S1) can be re-written into

$$Z = |Z|e^{j\phi} \quad (\text{S3})$$

where  $\phi$  represents the phase difference between applied AC voltage and the measured current. A pure resistor (with resistance  $R$ ) impedes the current that flows through it by a factor  $R$  while a capacitor impedes the current flow by a factor equal to the capacitive reactance  $X_c$ . When the resistance  $R$  and capacitance  $C$  are connected in parallel, the total complex impedance  $Z$  is given by<sup>8,9</sup>

$$\frac{1}{Z} = \left( \frac{1}{R} + j\omega C \right) \quad (\text{S4})$$

where  $\omega (= 2\pi f)$  is the varying frequency in rad/sec. Equation (S4) represents the complex impedance and can be simplified in the form of real and imaginary parts.

$$Z = \left( \frac{R}{1 + j\omega RC} \right) = \left( \frac{R}{1 + \omega^2 R^2 C^2} \right) - j \left( \frac{\omega CR^2}{1 + \omega^2 R^2 C^2} \right) \quad (\text{S5})$$

In the case of a contact resistance  $R_c$  in series with a parallel RC circuit (Fig. 1b) the complex impedance is given by Eqn (S6).

$$Z = \left( R_c + \frac{R}{1 + \omega^2 R^2 C^2} \right) - j \left( \frac{\omega CR^2}{1 + \omega^2 R^2 C^2} \right) \quad (\text{S6})$$

We performed  $J(V)$  measurements on molecular junctions of the form  $\text{Ag}^{\text{TS}}\text{-SC}_n\text{//GaO}_x\text{/EGaIn}$  and chose the junctions with electrical characteristics within one log-standard deviation of the mean values of  $J$  (which are reported in reference 1c) for the impedance measurements. We collected five impedance spectra with sMaRT (v3.2.1) software for each junction which was repeated for three junctions. The average data of all

data were used to fit with the equivalent circuit given in Fig. 1b using EIS spectrum analyser software. The EIS software uses a complex non-linear least squares fitting algorithm procedure developed by Boukamp.<sup>10</sup> The fitting was optimized for the equivalent circuit parameters by reducing the  $\chi^2$  value.

The frequency response is difficult to read out from the Nyquist plots directly. The Bode plots are often used to represent the frequency dependence of complex impedance. Figure S1 shows the Bode plots corresponding to the Nyquist plot in Fig. 3a.

**Figure S2.** The Bode plots for a junction with a SAM of SC<sub>10</sub> at various applied DC bias voltages.

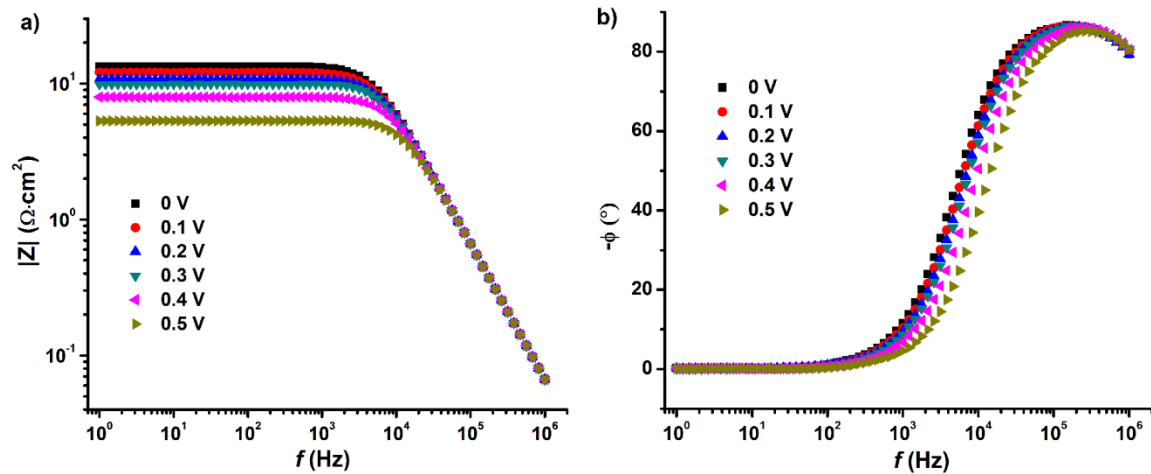
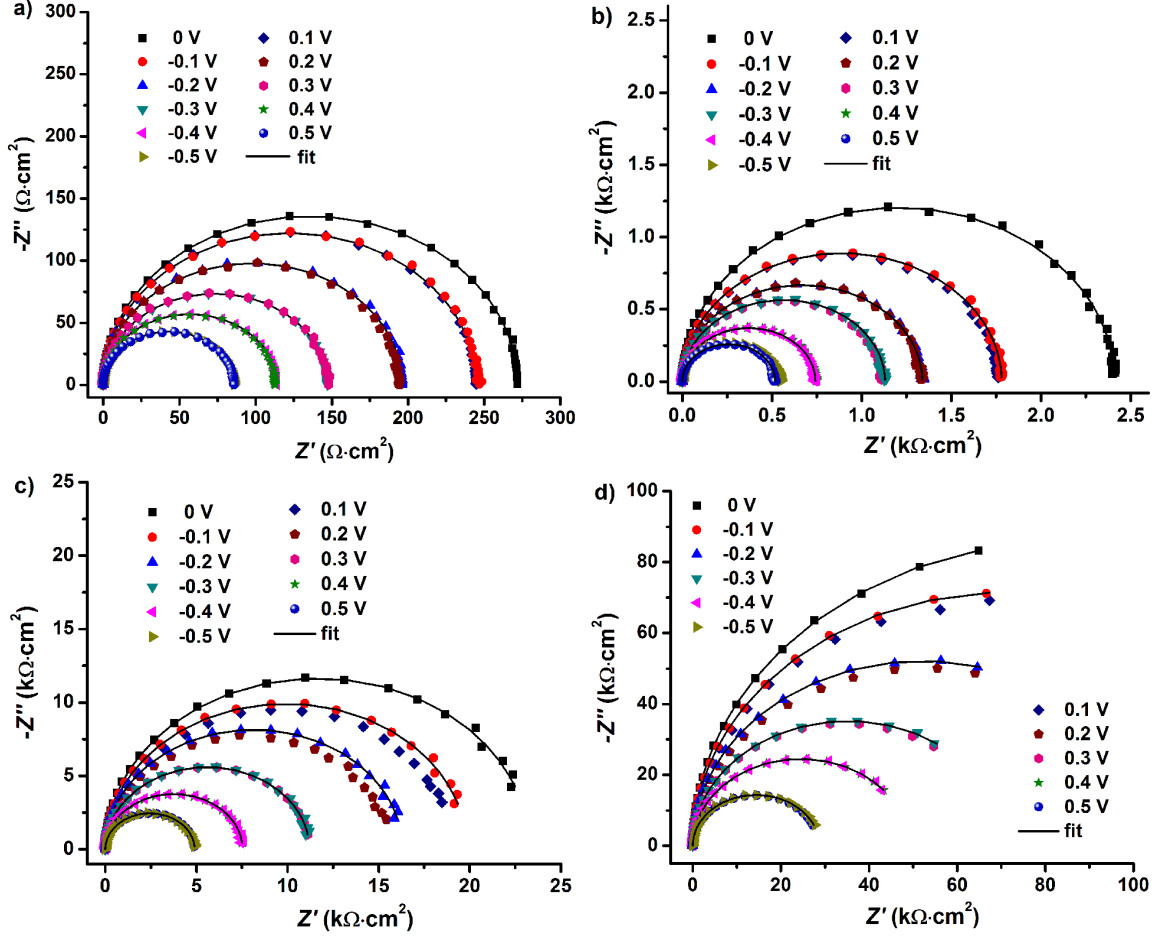


**Figure S3.** Nyquist plots for Ag<sup>TS</sup>-SC<sub>n</sub>//GaO<sub>x</sub>/EGaIn junctions with a)  $n = 12$ , b)  $n = 14$ , c)  $n = 16$  and d)  $n = 18$  at different applied DC bias voltages.



**Kramers-Kronig analysis.** Kramers-Kronig (KK) transforms are integral equations that form the real and imaginary components of complex quantities for systems which satisfy conditions of linearity, causality, and stability. These relations are very general expressions which can be applied to all frequency domain measurements to check the stability and linearity of the system. We used the KK-relations to validate our experimentally determined impedance. The KK transforms are given by<sup>8-10</sup>

$$Z'(\omega) = Z'(\infty) + (2/\pi) \int_0^{\infty} \frac{xZ''(x) - \omega Z''(\omega)}{x^2 - \omega^2} dx \quad (S7)$$

$$Z''(\omega) = (2/\pi) \int_0^{\infty} \frac{Z'(x) - Z'(\omega)}{x^2 - \omega^2} dx \quad (S8)$$

Fig. S4 shows the Kramers-Kronig plots for molecular junctions with SAMs of  $SC_n$  at various DC voltages. No obvious trends are visible and therefore we conclude that the data are linear and that the junctions did not change during the measurements. The measured impedance data are of good quality with acceptable signal-to-noise ratios.

**Figure S4:** Kramers-Kronig residual plots for  $Ag^{TS}-SC_n//GaO_x/EGaIn$  junctions at 0 V and 0.5 V DC bias voltages.

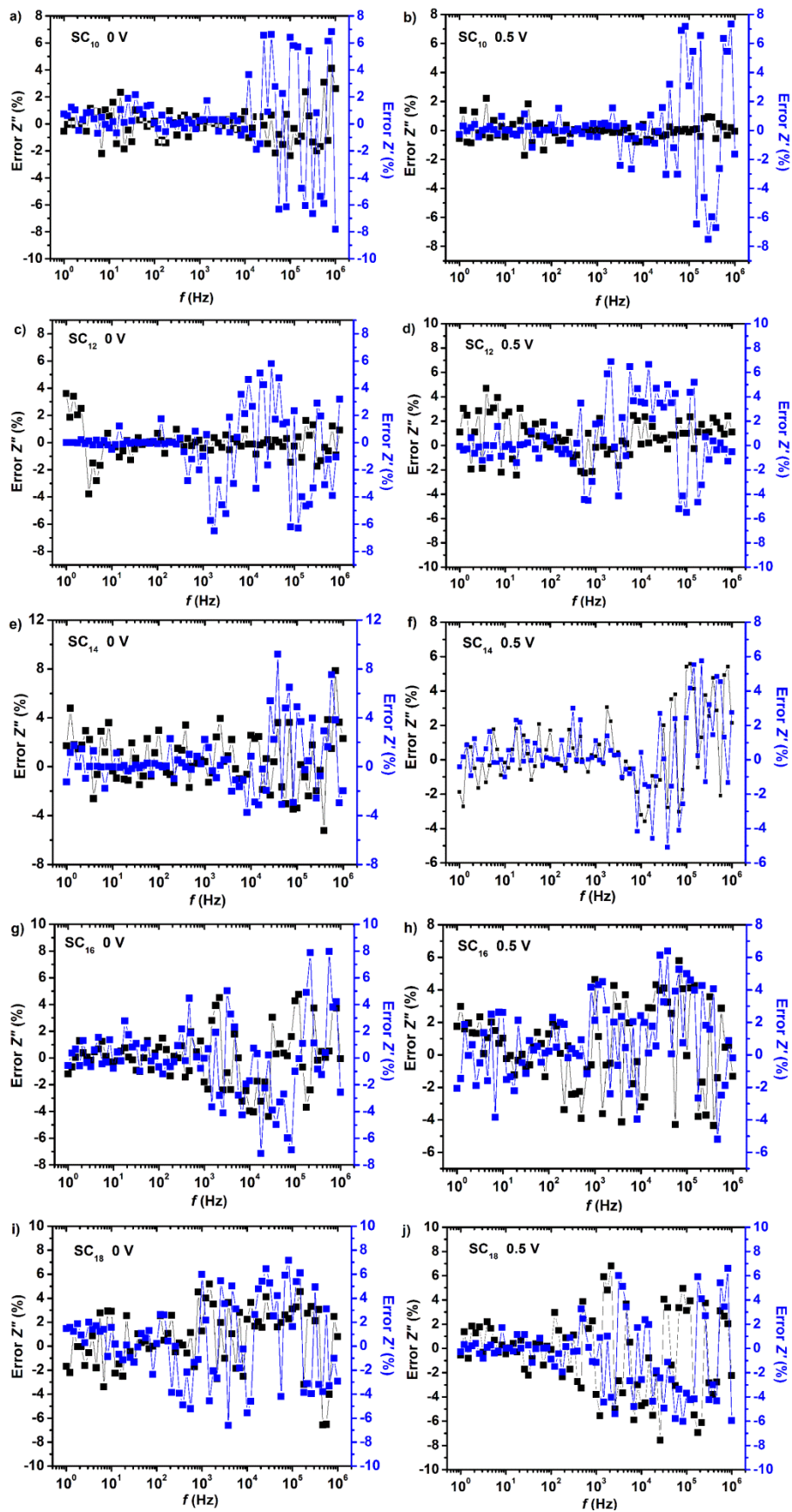
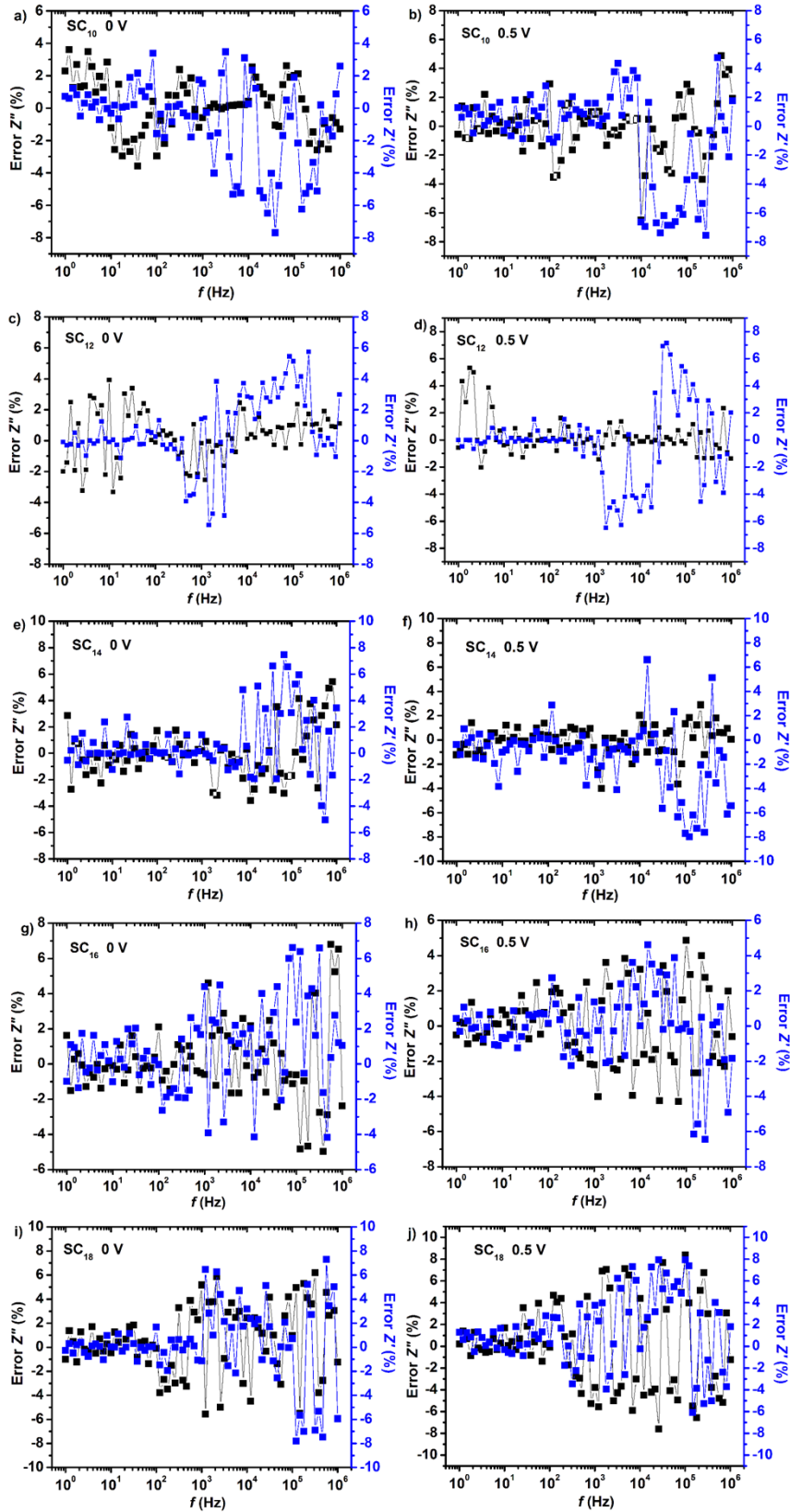


Figure S5: Residual plot for  $\text{Ag}^{\text{TS}}\text{-SC}_n\text{/GaO}_x\text{/EGaIn}$  junctions at 0 V and 0.5 V DC bias.



## Kramers-Kronig and Residual analysis

**Table S1:**  $\chi^2$  values at 0 V DC bias

SAM	$\chi^2_{\text{KK}}$	$\chi^2_{\text{fit}}$
SC <sub>10</sub>	0.0012	0.0015
SC <sub>12</sub>	0.001	0.0012
SC <sub>14</sub>	0.0014	0.0017
SC <sub>16</sub>	0.0014	0.0018
SC <sub>18</sub>	0.0015	0.0018

**Table S2:**  $\chi^2$  values at 0.5 V DC bias

SAM	$\chi^2_{\text{KK}}$	$\chi^2_{\text{fit}}$
SC <sub>10</sub>	0.0013	0.0014
SC <sub>12</sub>	0.0012	0.0014
SC <sub>14</sub>	0.0011	0.0014
SC <sub>16</sub>	0.0013	0.0015
SC <sub>18</sub>	0.0013	0.0017

**Resistance per molecule.** In SAM based molecular junctions, large numbers of molecules are connected in parallel between the two electrodes. Using the surface coverage of SAMs ( $\Gamma_{\text{SAM}} = 4.5 \times 10^{14}$  molecules/cm<sup>2</sup>) and assuming that all molecules have the same resistance with no charge transfer occurring in the lateral direction (i.e., from molecule to molecule), the resistance per molecule can be estimated as using eqn (S9) as reported previously by us.<sup>9</sup>

$$1/R_{\text{SAM}} = 1/r + 1/r + 1/r + L = n_{\text{mol}}/r = \Gamma_{\text{SAM}}/r \quad (\text{S9})$$

Figure S6 shows the resistance per molecule (corrected for the effective electrical contact area) obtained by us and those obtained by junctions based on conductive probe atomic force microscopy (CP-AFM for junctions)<sup>11</sup>, nano-particle AFM (NP-AFM)<sup>12</sup>, or scanning tunneling microscopy (STM) break-junctions experiments.<sup>13-15</sup> The difference between the CP-AFM experiments and the STM experiments can be explained as the

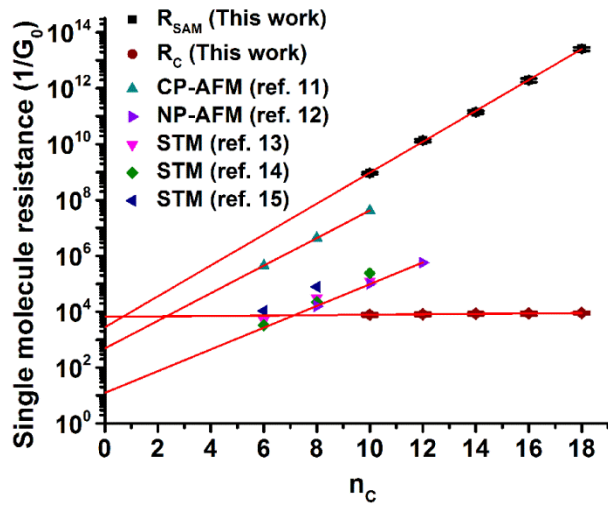
single molecule resistance of junctions with alkanedithiols (involving two chemisorbed molecule-metal contacts) is one to two orders smaller than that of junctions with alkanethiols (involving one chemisorbed and one physisorbed molecule-electrode contact as in EGaIn junctions). The NP-AFM experiments also involve two chemisorbed metal-molecule contacts and therefore the resistance is one to two orders smaller than that of junctions with alkanethiols. The single molecule resistance obtained from our EGaIn junctions is about one order of magnitude higher than that obtained from junctions with CP-AFM possibly due to the presence of the  $\text{GaO}_x$  layer or an error in the correction factor of the contact area.

Figure S6 also shows that extrapolation of the single molecule resistance to  $n_C = 0$  essentially yields  $R_C$ . Although this kind of extrapolation yields a resistance for a junction when  $n_C = 0$  that is associated with the contact resistance, we note that a “contact resistance” obtained in this way does depend on the applied bias<sup>16</sup> (and many other factors) and is perhaps only useful around zero bias (as shown here). We refer to eqn (3) in the main text where the distinction between contact resistance and the junction resistance is well-defined.

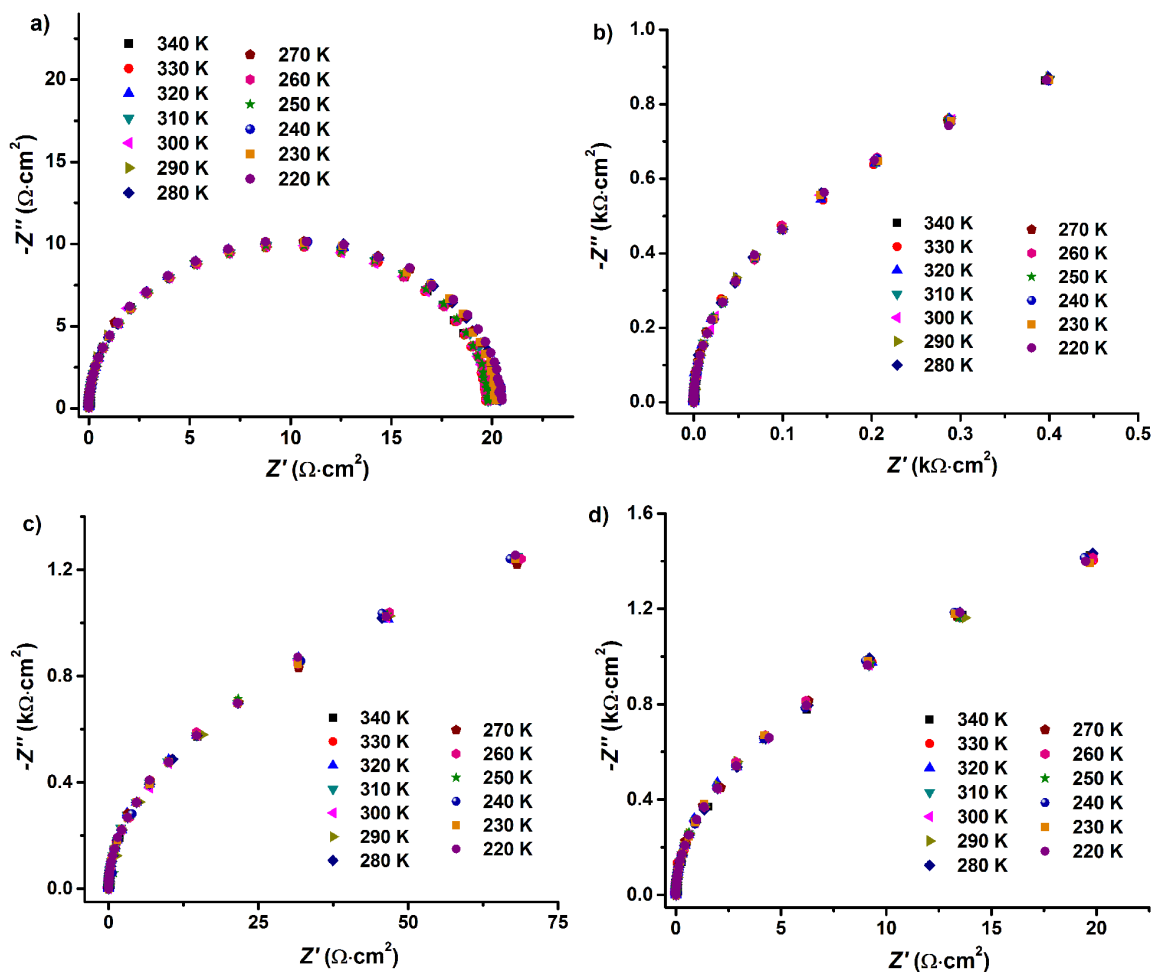
The values of the single molecule resistance of the EGaIn junctions reported here are one order in magnitude higher than the value reported in our previous paper. We note that this difference is due to the different experimental set-up we used. Here we used a highly sensitive impedance analyzer (model Solartron analytical 1260A) with 1296A dielectric interface, which enhances the input impedance of the impedance analyzer to 100 T $\Omega$ . Since the resistance of the SAMs measured are well below this limit (for example, the resistance of the junctions with a  $\text{SC}_{18}$  SAM are  $10^4$  times lower than the

limit), this new set up helps us to determine the impedance value more accurately than previously. In our previous measurements we used a LCR meter (model Wayne Kerr 43100) with limited input impedance of 100 M $\Omega$ . Since the values of the resistances of the junctions and the limit of the LCR meter are similar, the measured resistances underestimate the true resistances. Also by using the solartron impedance analyzer, we are able to measure frequency response down to 1 Hz which again improves the  $R_{SAM}$  value as resistance of the SAM dominates the low frequency part of the impedance spectra.

**Figure S6.** The single molecule resistances determined across several types of junctions.



**Figure S7.** Nyquist plot for Ag<sup>TS</sup>-SC<sub>n</sub>//GaO<sub>x</sub>/EGaIn junctions with a) n = 10, b) n = 14, c) n = 16 and d) n = 18 at various temperatures. The Nyquist plot axes are in different scales to show the semi-circular trend in the plots.



## References

1. Weiss, E. A.; Chiechi, R. C.; Kaufman, G. K.; Kriebel, J. K.; Li, Z. F.; Duati, M.; Rampi, M. A.; Whitesides, G. M., *J. Am. Chem. Soc.* 2007, **129**, 4336-4349.
2. Nerngchamng, N.; Yuan, L.; Qi, D.-C.; Li, J.; Thompson, D.; Nijhuis, C. A., *Nat. Nanotechnol.* 2013, **8**, 113-118.
3. Wan, A.; Jiang, L.; Sangeeth, C. S. S.; Nijhuis, C. A., *Adv. Fun. Mater.* 2014, **24**, 4442-4456.
4. Yuan, L.; Jiang, L.; Zhang, B.; Nijhuis, C. A., *Angew. Chem., Int. Ed.* 2014, **53**, 3377-3381.
5. Jiang, L.; Yuan, L.; Cao, L.; Nijhuis, C. A., *J. Am. Chem. Soc.* 2014, **136**, 1982-1991.
6. Hayes, G. J.; So, J. H.; Qusba, A.; Dickey, M. D.; Lazzi, G., *IEEE Tran. Antennas and Propagation* 2012, **60**, 2151-2156.
7. Dickey, M. D.; Chiechi, R. C.; Larsen, R. J.; Weiss, E. A.; Weitz, D. A.; Whitesides, G. M., *Adv. Fun. Mater.* 2008, **18**, 1097-1104.

8. Macdonald, J. R.; Johnson, W. B., Fundamentals of Impedance Spectroscopy. In *Impedance Spectroscopy*, John Wiley & Sons, Inc.: 2005; pp 1-26.
9. Sangeeth, C. S. S.; Wan, A.; Nijhuis, C. A., *J. Am. Chem. Soc.* 2014, **136**, 11134-11144.
10. Boukamp, B. A., *Solid State Ionics* 1986, **20**, 31-44.
11. Engelkes, V. B.; Beebe, J. M.; Frisbie, C. D., *J. Am. Chem. Soc.* 2004, **126**, 14287-14296.
12. Morita, T.; Lindsay, S., *J. Am. Chem. Soc.* 2007, **129**, 7262-7263.
13. Chen, F.; Li, X.; Hihath, J.; Huang, Z.; Tao, N., *J. Am. Chem. Soc.* 2006, **128**, 15874.
14. Li, C.; Pobelov, I.; Wandlowski, T.; Bagrets, A.; Arnold, A.; Evers, F., *J. Am. Chem. Soc.* 2008, **130**, 318.
15. Suzuki, M.; Fujii, S.; Fujihira, M., *Japan. J. Appl. Phys.* 2006, **45**, 2041.
16. Jiang, L.; Sangeeth, C. S. S.; Wan, A.; Vilan, A.; Nijhuis, C. A., *J. Phys. Chem. C* 2015, **119**, 960-969.